Inorg. Chem. **2009**, *48*, 1819−1825

Network Structured SnO_2/ZnO Heterojunction Nanocatalyst with High Photocatalytic Activity

Lirong Zheng,[†] Yuanhui Zheng,[*,‡] Chongqi Chen,[†] Yingying Zhan,[†] Xingyi Lin,[†] Qi Zheng,[*,†] Kemei Wei,[†] and Jiefang Zhu[§]

National Engineering Research Center of Chemical Fertilizer Catalyst, Fuzhou University, Gongye Road 523, Fuzhou 350002, Fujian, China, Department of Materials Engineering, Monash University, Clayton, 3800, VIC, Australia, and Department of Applied Physics, Chalmers University of Technology, Fysikgrand 3, Goteborg SE 412 96, Sweden

Received June 17, 2008

A network-structured SnO_2/ZnO heterojunction nanocatalyst with high photocatalytic activity was successfully synthesized through a simple two-step solvothermal method. The as-synthesized samples are characterized by X-ray diffraction, X-ray photoelectron spectroscopy, transmission electron microscopy, scanning electron microscopy, N_2 physical adsorption, and UV−vis spectroscopy. The results show that the SnO_2/ZnO sample with a molar ratio of Sn/Zn = 1 is a mesoporous composite material composed of SnO_2 and ZnO. The photocatalytic activity of SnO_2/ZnO heterojunction nanocatalysts for the degradation of methyl orange is much higher than those of solvothermally synthesized SnO_2 and ZnO samples, which can be attributed to the SnO_2−ZnO heterojunction, the pore structure, and higher Brunauer−Emmett−Teller (BET) surface area of the sample: (1) The SnO_2−ZnO heterojunction improves the separation of photogenerated electron−hole pairs due to the potential energy differences between SnO_2 and ZnO, thus enhancing the photocatalytic activity. (2) The SnO_2/ZnO sample might possess more surface reaction sites and adsorb and transport more dye molecules due to the higher BET surface area and many pore channels, also leading to higher photocatalytic activity.

1. Introduction

Recently, environmental problems such as air and water pollution have provided the impetus for sustained fundamental and applied research in the area of environmental remediation. Photocatalytic degradation of organic pollutants by using nanostructured semiconductors offers great potential for the complete elimination of toxic chemicals. It has been proven that the wide-bandgap semiconductor metal oxides (SMOs) such as TiO_2 and ZnO can degrade various organic pollutants under UV irradiation.[1−5] However, the fast recombination rate of the photogenerated electron−hole pairs hinders the industrial application of these semiconductors.[6] Therefore, suppression of the recombination of photogenerated electron−hole pairs in the semiconductors is essential for improving the efficiency of net charge transfer at the semiconductor−electrolyte interface.[7] In order to improve the charge separation in semiconductor systems, various SMO nanostructures with controllable oxygen or doping defects[4,8−10] and compositions (heterostructure)[11−16] have

* To whom correspondence should be addressed. Phone: +86-591-8373-1234-8112. Fax: +86-591-8373-8808. E-mail: yuanhui.zheng@eng.monash.edu.au (Y.Z.), zhengqi@fzu.edu.cn (Q.Z.).
† Fuzhou University.
‡ Monash University.
§ Chalmers University of Technology.

(1) Albu, S. P.; Ghicov, A.; Macak, J. M.; Hahn, R.; Schmuki, P. *Nano Lett.* **2007**, *7*, 1286.
(2) Dolamic, I.; Burgi, T. *J. Catal.* **2007**, *248*, 268.
(3) van der Meulen, T.; Mattson, A.; Osterlund, L. *J. Catal.* **2007**, *251*, 131.
(4) Zheng, Y.; Chen, C.; Zhan, Y.; Lin, X.; Zheng, Q.; Wei, K.; Zhu, J.; Zhu, Y. *Inorg. Chem.* **2007**, *46*, 6675.
(5) Xu, F.; Zhang, P.; Navrotsky, A.; Yuan, Z. Y.; Ren, T. Z.; Halasa, M.; Su, B. L. *Chem. Mater.* **2007**, *19*, 5680.
(6) Hoffmann, M. R.; Martin, S. T.; Choi, W. Y.; Bahnemann, D. W. *Chem. Rev.* **1995**, *95*, 69.
(7) Bedjat, I.; Kamat, P. V. *J. Phys. Chem.* **1995**, *99*, 9182.
(8) Nowotny, M. K.; Sheppard, L. R.; Bak, T.; Nowotny, J. *J. Phys. Chem. C* **2008**, *112*, 5275.
(9) Anandan, S.; Vinu, A.; Mori, T.; Gokulakrishnan, N.; Srinivasu, P.; Murugesan, V.; Ariga, K. *Catal. Commun.* **2007**, *8*, 1377.
(10) Zhou, J. K.; Lv, L.; Yu, J.; Li, H. L.; Guo, P. Z.; Sun, H.; Zhao, X. S. *J. Phys. Chem. C* **2008**, *112*, 5316.
(11) Zheng, Y.; Zheng, L.; Zhan, Y.; Lin, X.; Zheng, Q.; Wei, K. *Inorg. Chem.* **2007**, *46*, 6980.
(12) Kim, H. G.; Borse, P. H.; Choi, W.; Lee, J. S. *Angew. Chem., Int. Ed.* **2005**, *44*, 4585.

10.1021/ic802293p CCC: $40.75
Published on Web 02/05/2009

been successfully synthesized. Among these nanostructures, semiconductor-based heterostructure (i.e., metal/semiconductor and semiconductor/semiconductor heterostructure) nanocatalysts have received the most attention recently because of their excellent catalytic activity. For example, our previous research on Ag/ZnO heterostructure nanocatalysts shows that loading metallic Ag nanoparticles on the surface of ZnO nanorods can significantly enhance the photocatalytic activity,[11] and the dispersion of metallic Ag nanoparticles also affects the photocatalytic activity of the Ag/ZnO nanocatalyst.[17] In addition, semiconductor/semiconductor heterostructure photocatalysts may also increase the photocatalytic activity by extending the photoresponding range and increasing the charge separation rate, so a large variety of these heterostructures has been investigated and used for many photocatalytic reactions.[18−25] So far, there are two typical morphologies of semiconductor/semiconductor heterostructures, called "core/shell" and "non-core/shell" structures. In a core/shell structure system, one semiconductor is completely coated by the other semiconductor, so that only one of the charge carriers is accessible at the surface of the shell semiconductor, thus making selective charge transfer possible at the shell semiconductor−electrolyte interface. The other charge carrier gets trapped within the inner semiconductor and is not readily accessible. In a non-core/shell structure system, one semiconductor is only partially covered by the other semiconductor, so both electrons and holes are accessible to selective oxidation and reduction processes on their surfaces. Considering the higher utilization efficiency of separated charge carriers in non-core/shell structured semiconductor/semiconductor photocatalysts, the low cost of SnO_2 species, and the compatibility of some specific crystallographic planes of SnO_2 and ZnO nanocrystals,[26] we selected the SnO_2/ZnO system as target material and set out to synthesize non-core/shell structured SnO_2/ZnO heterojucntion nanocatalysts by using a simple method and, further, to understand the charge-transfer processes in this kind of multicomponent semiconductor system.

It has been reported that SnO_2/ZnO nanomaterials can be used as electrodes in lithium-ion batteries[27] and dye-sensitized solar cells,[28] sensors,[29,30] transistors,[31] and photocatalysts.[32−34] However, to the best of our knowledge, there is no research on the synthesis and photocatalysis of network-structured SnO_2/ZnO heterojunction nanocatalysts. In this work, a network-structured SnO_2/ZnO heterojunction photocatalyst was successfully synthesized through a simple two-step solvothermal method for the first time, in which solvothermally fabricated ZnO nanorods (named Z5 in ref 4) were used as seeds, and SnO_2 subsequently grew on their surfaces. In order to have an in-depth understanding of the relationship between the structure and photocatalytic activity, SnO_2, ZnO, and SnO_2/ZnO heterojunction nanocatalysts were investigated in detail. It is found that the SnO_2/ZnO material is a mesoporous composite material composed of SnO_2 and ZnO and exhibits excellent photocatalytic activity superior to the solvothermally synthesized SnO_2 and ZnO samples, which can be ascribed to the SnO_2−ZnO heterojunction, the pore structure, and a higher Brunauer−Emmett−Teller (BET) surface area of the sample.

2. Experimental Section

2.1. Preparation of SnO_2/ZnO Heterojunction Nanocatalyst. Materials. Zinc acetate, tin tetrachloride, sodium hydroxide, and alcohol were all of analytical grade and purchased from Shanghai Chemical Reagent, Ltd. without further purification.

Synthesis. A SnO_2/ZnO heterojunction nanocatalyst with a molar ratio of Zn/Sn = 1 was synthesized using a simple two-step solvothermal method. In a typical procedure, 1 mmol of $Zn(Ac)_2 \cdot 2H_2O$ and 5 mmol of NaOH were mixed in 30 mL of ethanol at room temperature with agitation for 30 min, then poured into a Teflon-lined stainless steel autoclave with a capacity of 50 mL. The sealed autoclave was put into an oven, heated to 160 °C, and maintained at this temperature for 24 h (first step). After the above reaction, 10 mL of a 0.1 M $SnCl_4$ aqueous solution was added into the autoclave with agitation. The sealed autoclave was put into an oven again, heated to 160 °C, and maintained at this temperature for another 24 h (second step). For comparison, SnO_2 was also synthesized using a solvothermal method: 10 mL of a 0.1 M $SnCl_4$

(13) Marci, G.; Augugliaro, V.; Lopez-Munoz, M. J.; Martin, C.; Palmisano, L.; Rives, V.; Schiavello, M.; Tilley, R. J. D.; Venezia, A. M. *J. Phys. Chem. B* **2001**, *105*, 1026. Marci, G.; Augugliaro, V.; Lopez-Munoz, M. J.; Martin, C.; Palmisano, L.; Rives, V.; Schiavello, M.; Tilley, R. J. D.; Venezia, A. M. *J. Phys. Chem. B* **2001**, *105*, 1033.

(14) Zhang, F.; Jin, R.; Chen, J.; Shao, C.; Gao, W.; Li, L.; Guan, N. *J. Catal.* **2005**, *232*, 424. Wu, J. J.; Tseng, C. H. *Appl. Catal., B* **2006**, *66*, 51.

(15) Lee, M. S.; Hong, S. S.; Mohseni, M. *J. Mol. Catal. A: Chem.* **2005**, *242*, 135. Iliev, V.; Tomova, D.; Todorovska, R.; Oliver, D.; Petrov, L.; Todorovsky, D.; Uzunova-Bujnova, M. *Appl. Catal., A* **2006**, *313*, 115.

(16) Lam, S. W.; Chiang, K.; Lim, T. M.; Amal, R.; Low, G. K.-C. *Appl. Catal., B* **2007**, *72*, 363.

(17) Zheng, Y.; Chen, C.; Zhan, Y.; Lin, X.; Zheng, Q.; Wei, K.; Zhu, J. *J. Phys. Chem. C* **2008**, *112*, 10773.

(18) Yang, J.; Li, D.; Wang, X.; Yang, X. J.; Lu, L. D. *J. Solid State Chem.* **2002**, *165*, 193.

(19) Shi, L. Y.; Li, C. Z.; Gu, H. C.; Fang, D. Y. *Mater. Chem. Phys.* **2000**, *62*, 62.

(20) Marci, G.; Augugliaro, V.; Lopez-Munoz, M. J.; Martin, C.; Palmisano, L.; Rives, V.; Schiavello, M.; Tilley, R. J. D.; Venezia, A. M. *J. Phys. Chem. B* **2001**, *105*, 1033.

(21) Bandara, J.; Tennakone, K.; Jayatilaka, P. P. B. *Chemosphere* **2002**, *49*, 439.

(22) Wang, C.; Zhao, J. C.; Wang, X. M.; Mai, B. X.; Sheng, G. Y.; Peng, P. A.; Fu, J. M. *Appl. Catal., B* **2002**, *39*, 269.

(23) Kwon, Y. T.; Song, K. Y.; Lee, W. I.; Choi, G. J.; Do, Y. R. *J. Catal.* **2000**, *191*, 192.

(24) Song, K. Y.; Park, M. K.; Kwon, Y. T.; Lee, H. W.; Chung, W. J.; Lee, W. I. *Chem. Mater.* **2001**, *13*, 2349.

(25) Pal, B.; Hata, T.; Goto, K.; Nogami, G. *J. Mol. Catal. A: Chem.* **2001**, *169*, 147.

(26) Kuang, Q.; Jiang, Z. Y.; Xie, Z. X.; Lin, S. C.; Lin, Z. W.; Xie, S. Y.; Huang, R. B.; Zheng, L. S. *J. Am. Chem. Soc.* **2005**, *127*, 11777.

(27) Belliard, F.; Irvine, J. T. S. *J. Power Sources* **2001**, *97*, 219.

(28) Ito, S.; Makari, Y.; Kitamura, T.; Wada, Y.; Yanagida, S. *J. Mater. Chem.* **2004**, *14*, 385.

(29) Yawale, S. P.; Yawale, S. S.; Lamdhade, G. T. *Sens. Actuators, A* **2007**, *135*, 388.

(30) Kim, K. W.; Cho, P. S.; Kim, S. J.; Lee, J. H.; Kang, C. Y.; Kim, J. S.; Yoon, S. J. *Sens. Actuators, B* **2007**, *123*, 318.

(31) McDowell, M. G.; Sanderson, R. J.; Hill, I. G. *Appl. Phys. Lett.* **2008**, *92*, 013502.

(32) Wang, W. W.; Zhu, Y. J.; Yang, L. X. *Adv. Funct. Mater.* **2007**, *17*, 59.

(33) Wang, C.; Zhao, J.; Wang, X.; Mai, B.; Sheng, G.; Peng, P.; Fu, J. *Appl. Catal., B* **2002**, *39*, 269.

(34) Dodd, A.; McKinley, A.; Saunders, M.; Tsuzuki, T. *Nanotechnology* **2006**, *17*, 692.

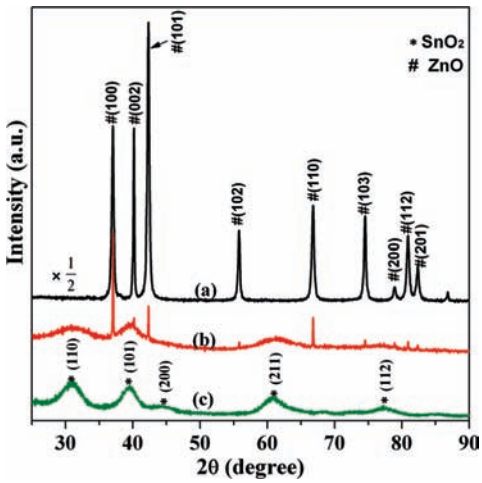

Figure 1. XRD patterns of the as-synthesized samples: (a) ZnO, (b) SnO_2/ZnO, and (c) SnO_2.

aqueous solution and 30 mL of a 0.17 M NaOH ethanol solution were mixed at room temperature and then poured into a Teflon-lined stainless steel autoclave with a capacity of 50 mL. The sealed reactor was heated to 160 °C and maintained at this temperature for 24 h. The final products were collected by filtration, washed with deionized water and ethanol several times, and finally dried in the air at 80 °C for 10 h.

2.2. Characterization. The powder X-ray diffraction (XRD) patterns of the samples were recorded by a PANalytical X' Pert Pro diffractometer with Co Kα radiation (λ = 0.179 nm) at a scanning rate of 0.12°/min. The X-ray photoelectron spectroscopy (XPS) measurements were performed on a Phi Quantum 2000 spectrophotometer with Al KR radiation (1486.6 eV; penetration depth of the X-ray: <10 nm). The microstructures and morphologies were investigated using a Tecnai G2 F20 field emission transmission electron microscope (TEM) working at 200 kV and a field emission scanning electron microscope (SEM, JSM-6700F) equipped with an energy-dispersive X-ray spectroscopy system working at 15 kV (penetration depth of the electrons: ~2.2 μm). To determine the textural properties of the as-prepared samples, N_2 adsorption/desorption measurements were carried out at 77 K using a Micrometrics ASAP 2020 system after the samples were degassed at 80 °C in a vacuum for 10 h. UV−vis diffuse-reflectance spectra of the as-synthesized samples were measured on a UV−vis−NIR spectrometer (Lambda 900). For photocatalytic measurements, 30 mg of each catalyst was suspended in 90 mL of a methyl orange (MO) aqueous solution (5.0×10^{-5} M), then placed in a quartz tube and agitated overnight in the absence of light to attain equilibrium adsorption on the catalyst surface. UV irradiation was carried out using a 2 × 4 W fluorescent Hg lamp (Philips TUV 4 W, the strongest emission at 254 nm). After a given irradiation time, about 3.5 mL of the mixture was withdrawn, and the catalysts were separated from the suspensions by filtration through 0.22 μm cellulose membranes. The photocatalytic degradation process was monitored using a UV−vis spectrophotometer (Lambda 950) measuring the absorption of MO at 463 nm.

3. Results and Discussion

The XRD patterns of the as-synthesized samples are shown in Figure 1. All diffraction peaks in Figure 1a and b are in good agreement with those of standard patterns for hexagonal wurtzite ZnO (JCPDS file no. 36-1451) and tetragonal rutile SnO_2 (JCPDS file no. 41-1445), respectively. The diffraction peaks of the ZnO nanocrystals (Figure 1a) are sharp and intense, revealing the highly crystalline character of the ZnO sample, while the diffraction peaks of the SnO_2 sample are broad and weak (Figure 1b), indicating a small crystal size or semicrystalline nature of this sample.[35] In Figure 1b, there are two sets of diffraction peaks for the SnO_2/ZnO sample, which are correspondingly ascribed to hexagonal wurtzite ZnO and tetragonal rutile SnO_2. No other characteristic peaks of SnO, $ZnSn(OH)_6$, $ZnSnO_3$, and Zn_2SnO_4 are detected in this sample, indicating that its composition is SnO_2 and ZnO. Comparing the full-width half-maximum of the SnO_2 semicrystalline peaks of the pure SnO_2 sample with that of the SnO_2/ZnO sample, one can conclude that the average grain size of SnO_2 semicrystals in the SnO_2/ZnO sample is a bit smaller than that of pure SnO_2. Furthermore, it is worthwhile to note that the diffraction peaks of ZnO nanocrystals in the SnO_2/ZnO sample are still very sharp despite the weak intensity, implying the highly crystalline character of ZnO nanocrystals in this sample.

The surface structure of the as-synthesized SnO_2/ZnO sample was investigated by XPS, and the corresponding experimental results are shown in Figure 2. In Figure 2a, all of the peaks on the curve are ascribed to Zn, Sn, O, and C elements, and no peaks of other elements are observed. The presence of C comes mainly from pump oil due to vacuum treatment before the XPS test. Figure 2b displays the high-resolution spectra for Zn and Sn species, respectively. The peak appearing in the upper part of Figure 2b is symmetric and centered at 1022.0 eV, which is attributed to the Zn $2p_{3/2}$ of Zn(II). And the peaks appearing in the lower part of Figure 2b are also symmetric and located at 486.8 and 495.2 eV, which are ascribed to the Sn $3d_{5/2}$ and Sn $3d_{3/2}$ of Sn(IV), respectively. On the basis of the above discussion, it is concluded that the SnO_2/ZnO sample is composed of Zn(II), Sn(IV), and O, in good agreement with the XRD result. In addition, the calculated Zn/Sn ratio is 0.18, indicating that most of the surface of the ZnO nanocrystals is covered by SnO_2 semicrystals (TEM and UV−vis diffuse-reflectance experiments further confirm this result and will be discussed later).

In order to obtain detailed information about the microstructure and morphology of the SnO_2/ZnO sample, SEM and TEM observations were carried out, and the results are shown in Figure 3. A typical SEM image (Figure 3a) shows that the SnO_2/ZnO sample is composed of nanoparticles with a size in the range of about 30−100 nm. Figure 3b is the energy-dispersive X-ray (EDX) spectrum from Figure 3a, further confirming that the SnO_2/ZnO sample is composed of Sn, Zn, and O, which is consistent with the XRD and XPS results (notice that the copper and carbon signals in Figure 3b are from the sample holder with conductive tape). EDX analysis reveals that the Zn/Sn ratio is 1.16:1, which is close to the theoretical Zn/Sn ratio (1:1). A low-magnified TEM image of the SnO_2/ZnO sample shows a network structure of SnO_2/ZnO consisting of multipod frameworks (highlighted by circles), as presented in Figure 3c. It is

(35) *X-ray Diffraction Procedure*; Klug, H.; Alexander, L., Eds.; Wiley: New York, 1962; p 125.

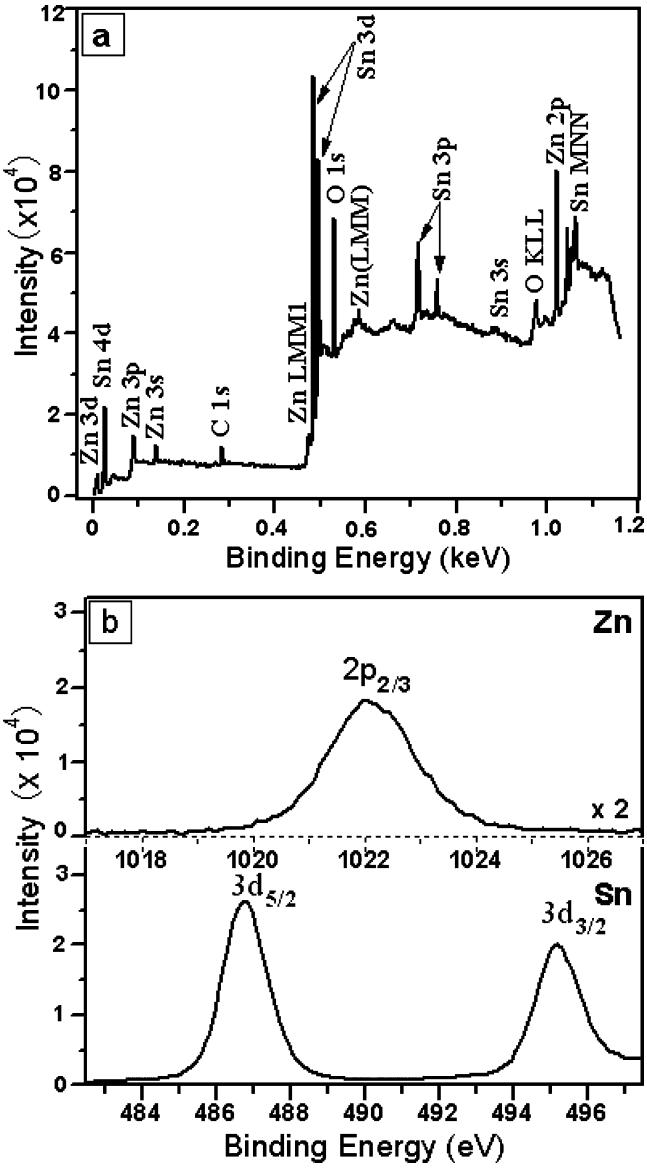

Figure 2. XPS patterns of the as-synthesized SnO_2/ZnO sample: (a) XPS full spectrum and (b) Zn $2p_{3/2}$ and Sn 3d spectra.

worthwhile to note that each nanoparticle attaches to several other nanoparticles and no self-nucleated and isolated SnO_2 or ZnO is observed, indicating the formation of a SnO_2−ZnO heterojunction. Moreover, the rodlike ZnO nanocrystals with a length of 100 nm[4] used as a starting material are also not observed in Figure 3c. In addition, one can see that the building blocks of the multipod framework have a uniform grain size of about 5−10 nm. A typical high-resolution TEM (HRTEM) image of a multipod framework is shown in Figure 3d. The uniform lattice structure and single-crystalline nature of the ZnO nanocrystal are observed in Figure 3d, and the spacings between adjacent lattice fringes are 0.26 and 0.28 nm, which are close to the *d*-spacings of the (002) and (100) planes, respectively, of hexagonal wurtzite ZnO. It is easy to find many holes with a size of about 3−5 nm on the surface of ZnO nanocrystals and some small pores (<5 nm) between nanaparticles (highlighted by circles), implying that the SnO_2/ZnO sample is mesoporous material. There are several semicrystalline nanoparticles on the surface

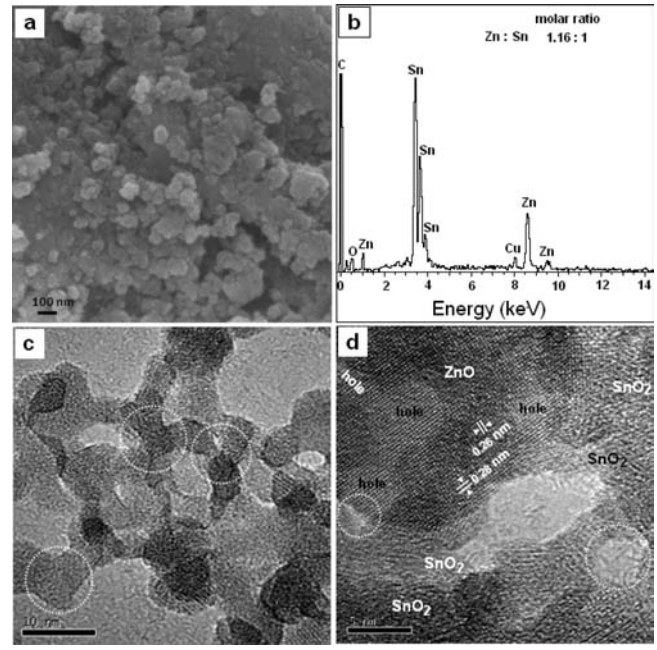

Figure 3. (a) SEM image of the as-synthesized SnO_2/ZnO heterojunction nanocatalyst, (b) EDX spectrum from Figure 3a, (c) TEM image, and (d) HRTEM image of the as-synthesized SnO_2/ZnO heterojunction nanocatalyst.

of the ZnO nanocrystal in Figure 3d, which are ascribed to SnO_2 semicrystals according to the XRD results. In addition, the exposed surface of the ZnO nanocrystal is easily observed in Figure 3d.

The texture of the as-synthesized SnO_2/ZnO sample was characterized by N_2 physisorption experiments. The N_2 adsorption−desorption isotherm and pore size distribution are shown in Figure 4. It can be seen from Figure 4a that the isotherm of the as-synthesized SnO_2/ZnO nanocatalyst is a type IV isotherm with a distinct H3 hysteresis loop in the range of 0.4−1.0 P/P_0 according to the IUPAC classification.[36] Its corresponding pore size distribution, calculated from the desorption branch of the N_2 isotherm by the Bopp−Jancso−Heinzinger method (in Figure 4b), shows that a narrow pore size distribution peak is centered at about 4.0 nm and a tailing peak is located between 5 and 11 nm, in good agreement with the TEM results (Figure 3c and d). Figure 4b shows that the dominant pore size of SnO_2/ZnO sample is 4.0 nm, confirming the mesoporous nature of this sample. The BET surface area of the SnO_2/ZnO sample is 168 m^2/g, which is much larger than those of pure SnO_2 (94 m^2/g) and ZnO (23 m^2/g).

The UV−vis diffuse-reflectance spectra of the as-synthesized samples are shown in Figure 5. The absorption edges of the as-synthesized SnO_2 semicrystals and ZnO nanorods[4] are located at about 305 and 380 nm, respectively, and it is obvious that there are two prominent absorption bands for the SnO_2/ZnO sample. The former is assigned to

(36) Sing, K. S. W. *Pure Appl. Chem.* **1982**, *54*, 2201.
(37) Mathew, X.; Enriquez, J. P.; Mejía-García, C.; Contreras-Puente, G.; Cortes-Jacome, M. A.; Toledo Antonio, J. A. *J. Appl. Phys.* **2006**, *100*, 073907.
(38) George, W. O.; McIntyre, P. S.; Mowthorpe, D. J. *Infrared Spectroscopy*; John Wiley & Sons Inc: New York, 1987; pp 21−40.

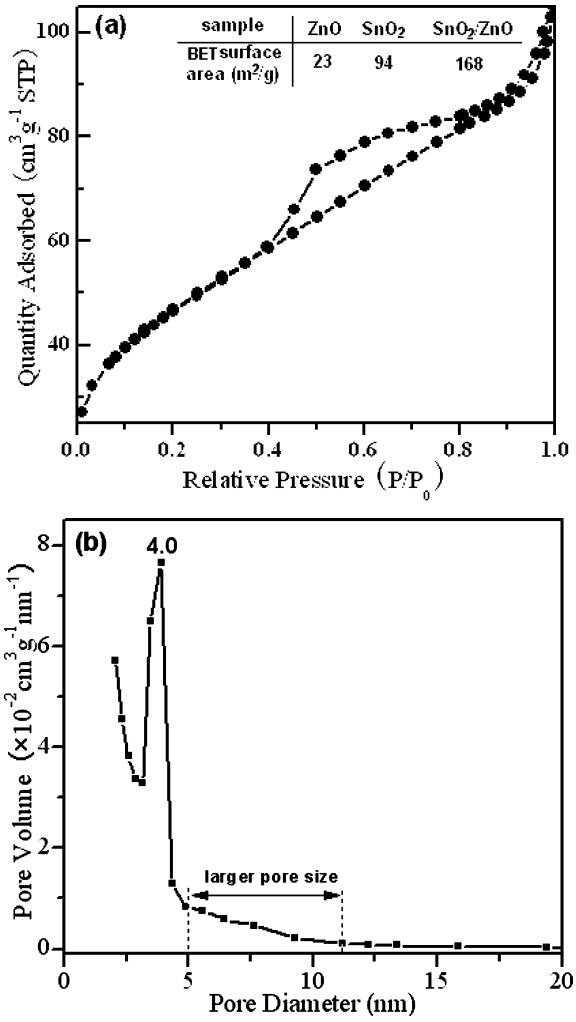

Figure 4. (a) Nitrogen adsorption−desorption isotherm and (b) pore size distribution of the as-synthesized SnO_2/ZnO heterojunction nanocatalyst.

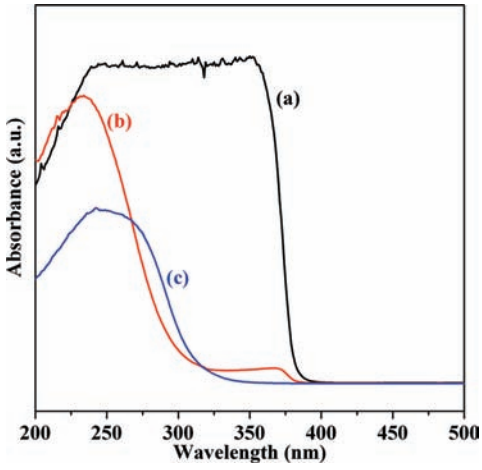

Figure 5. UV−vis diffuse-reflectance spectra of the as-synthesized samples: (a) ZnO, (b) SnO_2/ZnO, and (c) SnO_2.

the absorption of SnO_2 semicrystals, and the latter is attributed to the characteristic absorption of ZnO nanocrystals. The absorption edges of SnO_2 and ZnO nanocrystals in the SnO_2/ZnO sample shift blue slightly, indicating that the sizes of SnO_2 and ZnO in the SnO_2/ZnO sample are smaller than the corresponding value of pure SnO_2 or ZnO, which is in good agreement with the XRD results. The appearance

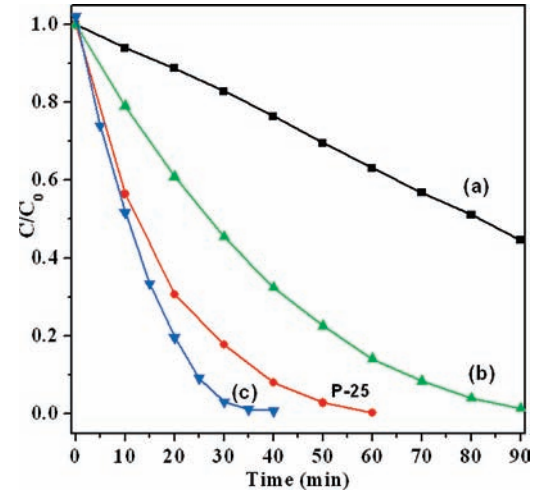

Figure 6. Photodegradation of MO by the as-synthesized samples: (a) SnO_2, (b) ZnO, and (c) SnO_2/ZnO nanocatalyst. The commercial TiO_2 (Degussa P-25) is used as a photocatalytic reference.

of two kinds of characteristic absorption bands also confirms that the SnO_2/ZnO sample is a composite material composed of SnO_2 and ZnO. For the SnO_2/ZnO sample, it is worthwhile to note that the absorption intensity of SnO_2 is much higher than that of ZnO, confirming that most of the surface of ZnO nanocrystals is covered by SnO_2 semicrystals.

MO was adopted as a representative organic pollutant to evaluate the photocatalytic performance of the as-synthesized photocatalysts. In the experiments, commercial TiO_2 (Degussa P-25) was used as a photocatalytic reference to qualitatively understand the photocatalytic activity of the SnO_2/ZnO heterojunction photocatalyst. The photocatalytic activities of the as-prepared samples and Degussa P-25 are shown in Figure 6. The degradation efficiency of the as-synthesized samples is defined as C/C_0, where C_0 and C are the initial concentration after the equilibrium adsorption and the reaction concentration of MO, respectively. As seen in Figure 6, the SnO_2/ZnO heterojunction catalyst shows the highest photocatalytic activity. In Figure 6a and b, the MO degradation efficiency is about 24% and 68% for pure SnO_2 and ZnO nanocrystals at 40 min, respectively. However, the required time for an entire decolorization of MO over the SnO_2/ZnO heterojunction catalyst (Figure 6c) is about 35 min, which is much shorter than the corresponding values of SnO_2, ZnO, and P-25 catalysts.

Figure 7 shows the proposed band structure of the as-synthesized SnO_2/ZnO heterojunction nanocatalyst.[17,39−41] When SnO_2 and ZnO form a heterojunction, their different work functions lead to the negatively charged carriers moving from SnO_2 (the material with low work function) to ZnO (the one with high work function) until their Fermi levels align (i.e., the system reaches the thermal equilibrium state); thus, an electrostatic field is created at the interface. At thermal equilibrium, the conduction band (CB) and valence band (VB) of SnO_2 and ZnO bend, and a depletion layer

(39) Robertson, J.; Xiong, K.; Clark, S. J. *Thin Solid Films* **2006**, *496*, 1.
(40) Sze, S. M.; Ng, K. K. *Physics of Semiconductor Devices*, 3rd ed.; John Wiley & Sons, Inc.: Hoboken, NJ, 2007.
(41) Könenkamp, R.; Word, R. C.; Godinez, M. *Nanotechnology* **2006**, *17*, 1858.

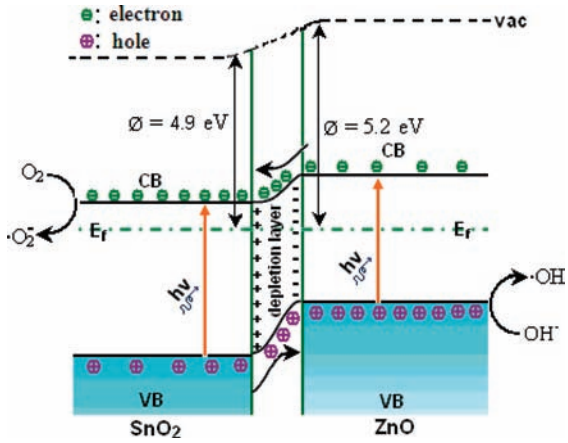

Figure 7. Energy-band diagram and photocatalytic mechanism of the as-aythesized SnO_2/ZnO heterojunction nanocatalyst. vac, vacuum level; Ef, Fermi level; CB, conduction band; VB, valence band.[17,39−41]

forms around the interface, too. When the SnO_2/ZnO catalyst is radiated by UV light with a photon energy higher or equal to the band gaps of SnO_2 and ZnO, electrons (e^-) in the VB can be excited to the CB with simultaneous generation of the same amount of holes (h^+) in the VB. The photogenerated electrons and holes are separated under the influence of the electrostatic field induced by different work functions. Thus, electrons move to the SnO_2 side and holes to the ZnO side. The photogenerated electrons and holes in the SnO_2/ZnO heterojunction nanocatalyst could inject into a reaction medium and participate in chemical reactions. For example, the electronic acceptors like adsorbed O_2 can easily trap the photoelectrons to produce a superoxide anion radical ($\cdot O_2^-$).[42] The role of O_2 during the photocatalytic process was investigated, and the results are shown in the Supporting Information (SI-1). It is found that O_2 is helpful for the degradation of MO, which can be ascribed to the formation of $\cdot O_2^-$. The formed $\cdot O_2^-$ might either attack organic molecules or provide hydroxyl radical species (·OH) by reacting with hydrion and photogenerated electrons.[43] The photoinduced holes can be easily trapped by OH^- to further produce a ·OH species, which is an extremely strong oxidant for the partial or complete mineralization of organic chemicals.[44] The following photocatalytic reactions possibly occur:

$$SnO_2/ZnO \xrightarrow{h\nu} SnO_2(e_{cb}^- \cdot\cdot h_{vb}^+)/ZnO(e_{cb}^- \cdot\cdot h_{vb}^+) \quad (1)$$

$$SnO_2(e_{cb}^- \cdot\cdot h_{vb}^+)/ZnO(e_{cb}^- \cdot\cdot h_{vb}^+) \rightarrow SnO_2 \cdot e_{cb}^-/ZnO \cdot h_{vb}^+ \quad (2)$$

$$SnO_2 \cdot e_{cb}^- + O_2(ad) \rightarrow SnO_2 + \cdot O_2^-(ad) \quad (3)$$

$$ZnO \cdot h_{vb}^+ + OH^- \rightarrow ZnO + \cdot OH \quad (4)$$

$$\cdot O_2^-(ad) \xrightarrow{H^+} HO_2^{\cdot} \xrightarrow[H^+]{e_{cb}^-} H_2O_2 \xrightarrow[\cdot O_2^-(ad)]{e_{cb}^- \text{ or}} \cdot OH + OH^- \quad (5)$$

$$MO + \cdot OH \rightarrow \text{degradation products} \quad (6)$$

On the basis of the above discussion, it is concluded, as follows, that (1) SnO_2 and ZnO in the SnO_2/ZnO heterojunction nanocatalyst not only serve as electron and hole sources (eq 1) but also act as a sink for the electrons and holes, respectively (eq 2); (2) the SnO_2−ZnO heterojunction promotes interfacial charge-transfer kinetics between SnO_2 and ZnO semiconductors and improves the separation of photogenerated electron−hole pairs (eq 2), thus enhancing the photocatalytic activity. Furthermore, the SnO_2/ZnO sample might possess more surface reaction sites and adsorb and transport more dye molecules due to the higher BET surface area and many pore channels, also leading to higher photocatalytic activity. In addition, when SnO_2 and ZnO grow together, there might be a very small amount of zinc and tin ions diffused into the other side. To understand the effect of diffused ions on the photocatalytic activity, a dilute HNO_3 solution was adopted to dissolve the ZnO nanocrystals in the SnO_2/ZnO sample, and the corresponding results are shown in the Supporting Information (SI-2). It is found that the BET surface area of the SnO_2/ZnO sample after the second cycle of HNO_3 treatment increases, while the photocatalytic activity decreases, revealing that the SnO_2−ZnO heterojunction has a positive effect on enhancing the photocatalytic activity. Only a small amount of ZnO nanocrystals in the SnO_2/ZnO sample cannot be dissolved, indicating that most of the ZnO and SnO_2 form a noncore/shell heterojunction; the insoluble Zn species might be ascribed to the ZnO nanocrystals fully covered by SnO_2 or the doped Zn^{2+} in SnO_2. Since we are not sure what the insoluble Zn species is, Zn^{2+}-doped SnO_2 was synthesized and studied (SI-2). It was found that Zn^{2+} ions in the lattice of SnO_2 can also enhance the photocatalytic activity. However, the contribution of the SnO_2/ZnO heterojunction to the photocatlytic activity is much greater than that of doped Zn^{2+} ions. Considering all of the above factors, it is reasonable that the SnO_2/ZnO heterojunction nanocatalyst has the highest photocatalytic activity in the as-synthesized samples. Finally, the results presented in this paper might be valuable for studying other semiconductor/semiconductor heterojunction catalysts.

4. Conclusion

Network-structured SnO_2/ZnO heterojunction nanocatalysts with high photocatalytic activity were successfully synthesized through a simple two-step solvothermal method. It was found that the SnO_2/ZnO nanocatalyst is a mesoporous composite material composed of SnO_2 and ZnO. The SnO_2/ZnO sample shows higher photocatalytic activity than pure SnO_2 and ZnO, which can be attributed to the SnO_2−ZnO heterojunction, the pore structure, and a higher BET surface area of the sample. The SnO_2−ZnO heterojunction improves the separation of photogenerated electron−hole pairs, thus enhancing the photocatalytic activity. Furthermore, the SnO_2/ZnO sample might possess more surface reaction sites and adsorb and transport more dye molecules due to the higher BET surface area and many pore channels, also leading to higher photocatalytic activity. The diffusion of a small

(42) Ryu, J.; Choi, W. *Environ. Sci. Technol.* **2004**, *38*, 2928.
(43) Marye, A. F.; Maria, T. D. *Chem. Rev.* **1993**, *93*, 341.
(44) Yatmaz, H. C.; Akyol, A.; Bayramoglu, M. *Ind. Eng. Chem. Res.* **2004**, *43*, 6035.

amount of Zn^{2+} ions into the SnO_2 may also facilitate an enhancement of the photocatalytic activity; a more detailed investigation about the effect of doped ions on the photocatlaytic activity is underway.

Acknowledgment. The authors acknowledge the financial support from the Department of Science of the People's Republic of China (20771025) and the Department of Science & Technology of Fujian Province (2005H201-2). The authors also thank Prof. Xiaohua Yang and Xiaokun Ding from the Instrumentation Analysis and Measurement Center of Fuzhou University for TEM measurement. Helpful comments by the reviewers are appreciated.

Supporting Information Available: Additional information and figures. This material is available free of charge via the Internet at http://pubs.acs.org.

IC802293P